Automated quantification of floating wood pieces in rivers from video monitoring: a new software tool and validation.

Hossein Ghaffarian[1, *], Pierre Lemaire[1,2], Zhang Zhi[1], Laure Tougne[2], Bruce MacVicar[3], and Hervé Piégay[1]

[1]Univ. Lyon, UMR 5600, Environnement-Ville-Société CNRS, F-69362 Lyon, France
[2]Univ. Lyon, UMR 5205, Laboratoire d'InfoRmatique en Image et Systèmes d'information CNRS, F-69676 Lyon, France
3Department of Civil and Environmental Engineering, Univ. Waterloo, Waterloo, Ontario, Canada

Correspondence to: Hossein Ghaffarian (hossein.ghaffarian@ens-lyon.fr)

Abstract

Wood is an essential component of rivers and plays a significant role in ecology and morphology. It can be also considered as a risk factor in rivers due to its influence on erosion and flooding. Quantifying and characterizing wood fluxes in rivers during floods would improve our understanding of the key processes but is hindered by technical challenges. Among various techniques for monitoring wood in rivers, streamside videography is a powerful approach to quantify different characteristics of wood in rivers, but past research has employed a manual approach that has many limitations. In this work, we introduce new software for the automatic detection of wood pieces in rivers. We apply different image analysis techniques such as static and dynamic masks, object tracking, and object characterization to minimize false positive and missed detections. To assess the software performance, results are compared with manual detections of wood from the same videos, which was a time-consuming process. Key parameters that affect detection are assessed including surface reflections, lighting conditions, flow discharge, wood position relative to the camera, and the length of wood pieces. Preliminary results had a 36% rate of false positive detection, primarily due to light reflection and water waves, but post-processing reduced this rate to 15%. The missed detection rate was 71% of piece numbers in the preliminary result, but post processing reduced this error to only 6.5% of piece numbers, and 13.5% of volume. The high precision of the software shows that it can be used to massively increase the quantity of wood flux data in rivers around the world, potentially in real time. The significant impact of post-processing indicates that it is necessary to train the software in various situations (location, timespan, weather conditions) to ensure reliable results. Manual wood detections and annotations for this work took more than one human-month of labor. In comparison, the presented software coupled with an appropriate post pro-cessing step performed the same task in real time (55 hr) on a standard desktop computer.

Keywords: River monitoring, Wood flux, Wood discharge, Large wood, Ground video imagery, Automatic detection

1. Introduction

Floating wood has a significant impact on river morphology (Gurnell et al., 2002; Gregory et al., 2003; Wohl, 2013; Wohl and Scott, 2017). It is both a component of stream ecosystems and a source of risk for human activities (Comiti et al., 2006; Badoux et al., 2014; Lucía et al., 2015). The deposition of wood at given locations can cause a reduction of the cross-sectional area, which can both increase upstream water levels (and the risk for neighboring communities), and laterally concentrate the flow downstream, which can lead to damaged infrastructure (Lyn et al., 2003; Lagasse, 2010; Mao and Comiti, 2010; Badoux et al., 2014; Ruiz-Villanueva et al., 2014; De Cicco et al., 2018; Mazzorana et al., 2018). Therefore, understanding and monitoring the dynamics of wood within a river is fundamental to assess and mitigate risk. An important body of work on this topic has grown over the last two decades, which has led to the development of many monitoring techniques (Marcus et al., 2002; MacVicar et al., 2009a; MacVicar and Piégay, 2012; Benacchio et al., 2015; Ravazzolo et al., 2015; Ruiz-Villanueva et al., 2018; Ghaffarian et al., 2020; Zhang et al., 2020) and conceptual and quantitative models (Braudrick and Grant, 2000; Martin and Benda, 2001; Abbe and Montgomery, 2003; Gregory et al., 2003; Seo and Nakamura, 2009; Seo et al., 2010). A recent review by Ruiz-Villanueva et al. (2016), however, argues that the area remains in relative infancy compared to other river processes such as the characterization of channel hydraulics and sediment transport. Many questions remain open areas of inquiry including wood hydraulics, which is needed to understand wood recruitment, movement and trapping, and wood budgeting, where better parametrization is needed to understand and model the transfer of wood in watersheds at different scales.

In this domain, the quantification of wood mobility and wood fluxes in real rivers is a fundamental limitation that constrains model development. Most early works were based on repeated field surveys (Keller and Swanson, 1979; Lienkaemper and Swanson, 1987), with more recent efforts taking advantage of aerial photos or satellite images (Marcus et al., 2003; Lejot et al., 2007; Lassettre et al., 2008; Senter and Pasternack, 2011; Boivin et al., 2017) to estimate wood delivery at larger time scales of 1 year up to several decades. Others have monitored wood mobility once introduced by tracking wood movement in floods (Jacobson et al., 1999; Haga et al., 2002; Warren and Kraft, 2008). Tracking technologies such as active and passive Radio Frequency Identification transponders (MacVicar et al., 2009a; Schenk et al., 2014) or GPS emitters and

receivers (Ravazzolo et al., 2015) can improve the precision of this strategy. To better understand wood flux, specific trapping structures such as reservoirs or hydropower dams can be used to sample the flux over time interval windows (Moulin and Piégay, 2004; Seo et al., 2008; Turowski et al., 2013). Accumulations upstream of a retention structure can also be monitored where they trap most or all of the transported wood, as was observed by Boivin *et al.* (2015), to quantify wood flux at the flood event or annual scale. All these approaches allow the assessment of wood budget and the in-channel wood exchange between geographical compartments within a given river reach and over a given period (Schenk et al., 2014; Boivin et al., 2015, 2017).

For finer scale information on the transport of wood during flood events, video recording of the water surface is suitable for estimating instantaneous fluxes and size distributions of floating wood in transport (Ghaffarian et al., 2020). Classic monitoring cameras installed on the river bank are cheap and relatively easy to acquire, setup and maintain. As is seen in Table 1, a wide range of sampling rates and spatial/temporal scales have been used to assess wood budgets in rivers. MacVicar and Piégay (2012) and Zhang et al., (2020) (in review), for instance, monitored wood fluxes at 5 frames per second (fps) and a resolution of 640 × 480 up to 800 × 600 pixels. Boivin et al. (2017) used a similar camera and frame rate as MacVicar and Piégay (2012) to compare periods of wood transport with and without the presence of ice. Senter et al. (2017) analyzed the complete daytime record of 39 days of videos recorded at 4 fps and a resolution of 2048 × 1536 pixels. Conceptually similar to the video technique, time-lapse imagery can be substituted when large rivers where surface velocities are low enough and the field of view is large. Kramer and Wohl (2014); Kramer et al. (2017) applied this technique in the Slave River (Canada) and recorded one image every 1 and 10 minutes. Where possible, wood pieces within the field of view are then visually detected and measured using simple software to measure the length and diameter of the wood to estimate wood flux (piece/s) or wood volume (m^3/s) (MacVicar and Piégay, 2012; Senter et al., 2017). Critically for this approach, the time it takes for the researchers to extract information about wood fluxes has limited the fraction of the time that can be reasonably analyzed. Given the outdoor location for the camera, the image properties depend heavily on lighting conditions (e.g. surface light reflections, low light, ice, poor resolution or surface waves) which may also limit the accuracy of frequency and size information (Muste et al., 2008; MacVicar et al., 2009a). In such situations, simpler metrics such as a count of wood pieces, a classification of wood transport intensity, or even just a binary presence/absence may be used to characterize the wood flux (Boivin et al., 2017; Kramer et al., 2017).

Table 1

A fully automatic wood detection and characterization algorithm can greatly improve our ability to exploit the vast amounts of data on wood transport that can be collected from streamside video cameras. From a computer science perspective, however, automatic detection and characterization remain challenging issues. In computer vision, detecting objects within videos typically consists of separating the foreground (the object of interest) from the background (Roussillon et al., 2009; Cerutti et al., 2011, 2013). The basic hypothesis is that the background is relatively static and covers a large part of the image, allowing it to be matched between successive images. In the riverine environments, however, such an assumption is unrealistic because the background shows a flowing river, which can have rapidly fluctuating properties (Ali and Tougne, 2009). Floating objects are also partially submerged in water that has high suspended material concentrations during floods, making them only partially visible (*e.g.* a single piece of wood may be perceived as multiple objects) (MacVicar et al., 2009b). Detecting such an object in motion within a dynamic background is an area of active research (Ali et al., 2012, 2014; Lemaire et al., 2014; Piégay et al., 2014; Benacchio et al., 2017). Accurate object detection typically relies on the assumption that objects of a single class (e.g. faces, bicycles, animals, etc.) have a distinctive aspect or set of features that can be used to distinguish between types of objects. With the help of a representative dataset, machine learning algorithms aim at defining the most salient visual characteristics of the class of interest (Lemaire et al., 2014; Viola and Jones, 2006). When the objects have a wide intra-class aspect range, a large amount of data can compensate by allowing the application of deep learning algorithms (Gordo et al., 2016; Liu et al., 2020). To our knowledge, such a database is not available in the case of floating wood.

The camera installed on the Ain River in France has been operating more or less continuously for over 10 years and vast improvements in data storage mean that this data can be saved indefinitely (Zhang et al., 2020). The ability to process this image database to extract the wood fluxes allows us to integrate this information over floods, seasons and years, which would allow us to significantly advance our understanding of the variability within and between floods over a long time period. An unsupervised method to identify floating wood in these videos by applying intensity, gradient and temporal masks was developed by Ali and Tougne (2009) and Ali *et al.* (2011). In this model, the objects were tracked through the frame to ensure that they followed the direction of flow. An analysis of about 35 minutes of the video showed that approximately 90% of the wood pieces was detected (*i.e.* about 10% of detection were missed), which confirmed the potential utility of this approach. An additional set of false detection related to surface wave conditions amounted to approximately 15% of the total detection. However, the developed algorithm was not always stable and

was found to perform poorly when applied to a larger data set.

The objectives of the presented work are to describe and validate a new algorithm and computer interface for quantifying floating wood pieces in rivers. First, the algorithm procedure is introduced to show how wood pieces are detected and characterized. Second, the computer interface is presented to show how manual annotation is integrated with the algorithm to train the detection procedure. Third, the procedure is validated using data from the Ain River. The validation period occurred over six days in January and December 2012 where flow conditions ranged from $\sim 400\ m^3/s$, which is below bankfull discharge but above the wood transport threshold, to more than $800\ m^3/s$. The developed algorithm can be used to characterize wood pieces for a large image database at the study site. Future applications of this approach at a wide range of sites should lead to new insights on the variability of wood pieces at the reach and watershed scales in world rivers.

2. Methodological procedure for automatic detection of wood

The algorithm for wood detection comprises a number of steps that seek to locate objects moving through the field of view in a series of images and then identify the objects most likely to be wood. The algorithm used in this work modifies the approach described by Ali *et al.*, (2011). The steps work from a pixel to image to video scale, with the context from the larger scale helping to assess whether the information at the smaller scale indicates the presence of floating wood or not. In a still image, a single pixel is characterized by its location within the image, its color and its intensity. Looking at its surrounding pixels, on an image scale, allows that information to be spatially contextualized. Meanwhile, the video data adds temporal context, so that previous and future states of a given pixel can be used to assess its likeliness of representing floating wood. Since an image is only a discrete 2D representation of the real 3D world, details about the camera parameters such as optical image deformations, geographic situation, perspective deformations or behavior regarding luminosity can be used to infer what wood should look like and where it should occur. On a video scale, the method can embed expectations about how wood pieces should move through frames, how big they should be, and how lighting and weather conditions can evolve to change the expectations of wood appearance, location, and movement. The specific steps followed by the algorithm are shown in a simple flow chart (Fig 1.a). An example image with a wood piece in the middle of the frame is also shown for reference (Fig 1.b).

Fig 1

2.1. Wood probability masks

In the first step, each pixel was analyzed individually and independently. The static probability mask answers the question "is one pixel likely to belong to a wood-block, given its color and intensity?". The algorithm assumes that the wood pixels can be identified by pixel light intensity (x) following a Gaussian distribution (Fig 2.a). To set the algorithm parameters, manual annotations of wood are used to obtain a representative sample of wood pixels, from which both the mean (μ) and standard deviation (σ) are calculated. This procedure produces a static probability mask (Fig 2.b). From this figure, it is possible to identify the sectors where wood presence is likely, which includes the floating wood piece seen in Fig 1.b, but also includes standing vegetation in the lower part of the image and a shadowed area in the upper left. The advantage of this approach is that it is computationally very fast. However, misclassification is possible, particularly when light condition changes.

Fig 2

The second mask, called the dynamic probability mask, outlines each pixel's recent history. The corresponding question is: "is this pixel likely to represent wood now, given its past and present characteristics?". Again, this step is based on what is most common in our database: it is assumed that a wood pixel is darker than a water pixel. Depending on lighting conditions like shadows cast on water or waves, this is not always true, i.e. water pixels can be as dark as wood pixels. However, pixels displaying successively water then wood tend to become immediately and significantly darker, while pixels displaying wood then water tend to become significantly lighter. Meanwhile, pixels that keep on displaying wood tend to be rather stable. Thus, we assign wood pixel probability according to an updated version of the function proposed by Ali et al. (2011) (Fig 3.a) that takes 4 parameters. This function H is an updating function, which produces a temporal probability mask from the inter-frame pixel value. On a probability map, a pixel value ranges from -1 (likely not wood) to 1 (likely wood). The temporal mask value for a pixel at location (x, y) and at time t is $P_T(x, y, t) = H(\Delta_t, I) + P_T(x, y, t-1)$. We apply a threshold to the output of $P_T(x, y, t)$ so that it always stays within the interval $[0,1]$. The idea is that a pixel that becomes suddenly and significantly darker is assumed to be likely wood. $H(\Delta_t, I)$ is such that under those conditions, it increases the pixel probability map value (parameters τ and β). A pixel that becomes lighter over time is unlikely to correspond to wood (parameter α). A pixel which intensity is stable and that was previously assumed to be wood shall still correspond to wood, while a pixel which intensity is stable and which probability to be wood was low is unlikely to represent wood now. A small decay factor (δ) was introduced in order to prevent divergence (in particular,

it prevents noisy areas from being activated too frequently).

Fig 3

The final wood probability mask is created using a combination of both the static and dynamic probability masks. Wood objects thus had to have a combination of the correct pixel color and the expected temporal behavior of water-wood-water color. The masks were combined assuming that both probabilities are independent, which allowed us to use the Bayesian probability rule in which the probability masks are simply multiplied, pixel by pixel, to obtain the final probability value for each pixel of every frame.

2.2. Wood object identification and characterization

From the probability mask it is necessary to group pixels with high wood probabilities into objects and then to separate these objects from the background to track them through the image frame. For this purpose, pixels were classified as high-or low-probability based on a threshold applied to the combined probability mask. Then, the high-probability pixels were grouped into connected components (that is, small, contiguous regions on the image) to define the objects. At this stage, a pixel size threshold was applied on the detected objects so that only the bigger objects were considered to represent woody objects on the water surface (Fig 4.a the big white region at the middle). A number of smaller components were often related to non-wood objects, for example waves, reflections, or noise from the camera sensor or data compression.

After the size thresholding step, movement direction and velocity were used as filters to distinguish real objects from false detections. The question here is, "is this object moving through the image frame the way we would expect floating wood to move?". To do this, the spatial and temporal behavior of components were analyzed. First, to deal with partly immersed objects, we agglomerated multiple objects within frames as components of a single object if the distance separating them was less than a set threshold. Second, we associated wood objects in successive frames together to determine if the motion of a given object was compatible with what is expected from driftwood. This can be achieved according to the dimensionless parameter "$PT/\Delta T$", which provides a general guideline for the distance an object pass between two consecutive frames (Zhang et al., 2020). Here PT (passing time) is the time that one piece of wood passes through the camera field of view and ΔT is the time between two consecutive frames and practically it is recommended to use videos with $PT/\Delta T > 5$ in this software. In our case, tracking wood is rather difficult for classical object tracking approaches in computer vision: the background is very noisy, the acquisition frequency is low and the objects appearance can be highly variable due to temporarily submerged parts and highly variable 3D

structures. Given these considerations it was necessary to use very basic rules for this step. The rules are therefore based on loose expectations, in terms of pixel intervals, on the motions of the objects, depending on the camera location and the river properties. How many pixels is the object likely to move between image frames from left to right? How many pixels from top to bottom? How many appearances are required? How many frames can we miss because of temporary immersions? Using these rules, computational costs remained low and the analysis could by run in real-time while also providing good performance.

Fig 4

The final step was to characterize each object, which at this point in the process are considered wood objects. Each appears several times in different frames and a procedure is needed to either pick a single representative occurrence or use a statistic tool to analyse multiple occurrences to estimate characterization data. Here we assumed that the biggest occurrence, in terms of pixels number, was the most representative state. This assumption is based on the principle that a bigger number of pixels corresponds to a better or a fuller view (the object is less immersed than on other occurrences, for instance). This approach also matched the manual annotation procedure where we tended to pick the view where the object covers the largest area to make measurements. For the current paper, every object as characterized from the raw image based on its size and its location (in pixels).

2.3. Image rectification

Warping images according to a perspective transform results in an important loss of quality. On warped images, areas of the image farther to the camera provide little detail and are overall very blurry and non-informative. Therefore, given the topology of our images, image rectification was necessary to calculated wood length, velocity, volume and other characteristics from the saved pixel-based characterization of each object. To do so, the fisheye lens distortion was first corrected. A fisheye lens distortion is a characteristic of the lens that produces visual distortion intended to create a wide panoramic or hemispherical image. This effect was corrected by a standard Matlab process using the ComputerVisionToolbox^{TM}.

Ground-based cameras have also an oblique angle of view, which means that pixel to meter correspondence is variable and images need to be orthorectified to obtain estimates of object size and velocity in real terms (Muste et al., 2008). Orthorectification refers to the process by which image distortion is removed and the image scale is adjusted to match the actual scale of the water surface. Translating from pixels to cartesian coordinates required us to assume that our camera follows the pinhole camera model and that the river can

be assimilated to a plane of constant altitude. Under such conditions, it is possible to translate from pixel coordinates to a metric 2D space thanks to a perspective transform assuming a virtual pinhole camera on the image and estimating the position of the camera and its principal point (center of the view). An example of orthorectification on a detected wood piece in a set of continuous frames and pixel coordinates (Fig 5.b) is presented in Fig 5.c in metrics coordinates. The transform matrix is obtained with the help of at least 4 non-colinear points (Fig 5.a blue GCPs (Ground Control Points) acquired with DGPS) from which we know both the relative 2D metric coordinates for a given water level (Fig 5.c blue points), and their corresponding localization within the image(Fig 5.b blue points). To achieve better accuracy, it is advised to acquire additional points and to solve the subsequent over-determined system with the help of a Least Square Regression (LSR). Robust estimators such as RANSAC can provide useful to prevent acquisition noise. After identifying the virtual camera position, the perspective transform matrix then becomes parameterized with the water level. Handling the variable water level was performed for each piece of wood, by measuring the relative height between the camera and the water level at the time of detection based on information recorded at the gauging station to which the camera was attached.

Fig 5

3. User interface

The software was developed to provide a single environment for the analysis of wood pieces on the surface of the water from streamside videos. It consists of four distinct modules: Detection, Annotation, Learning, and Performance. The home screen (Fig 6) allows the operator to select any of these modules. From within a module, a menu bar on the left side of the interface allows operators to switch from one module to another. In the following sections, the operation of each of these modules are described.

Fig 6

3.1. Detection

The detection module is the heart of the software. This module allows, from learned or manually specified parameters, the detecting of floating objects without human intervention (see Fig 7). This module contains two main parts: (i) Detection tab, which allows operator to open, analyze and export the results from one video or a set of videos, and (ii) Configuration tab, which allows operator to load and save the software configuration by defining the parameters of wood detection (as described in Sect 2), saving and extracting the results, and displaying the interface.

The detection process is intended to work as a video file player. The idea is to load a video file (or a stream url), and to let the software read the video until the end. When required, the reader generates a visual output, showing how the masks behave by adding color and information to the video content (see Figure 7). A small textual display area shows the frequency of past detections. Meanwhile, the software generates a series of files summarizing the positive outputs of the detection. They consist in YAML and CSV files, as well as image files to show the output of different masks, the original frames, etc. A configuration tab is available, and provides many parameters organized by various categories. The main configuration tab is divided in seven parts. The first part is dedicated to general configurations such as frame skipped between each computation and defining the areas within the frame where wood is not expected (e.g. bridge pier or river bank). In the second and third parts, the parameters of the intensity and temporal masks are listed (see Sect 2.1). The default values are $\mu = 0.2$ and $\sigma = 0.08$ for the intensity mask, and $\tau = 0.25$ and $\beta = 0.45$ for the temporal mask. In the fourth and fifth parts, object tracking and characterization parameters are defined respectively as described in Sect 2.2. Detection time is defined in the sixth part using an optical character recognition technique. Finally, the parameters of the orthorectification (see Sect 2.3) are defined in the seventh part. The detection software can be used to process videos in batch ("script" tab), without generating a visual output to save computing resources.

Fig 7

3.2. Annotation

As mentioned in Sec. 2, the detection procedure requires the classification of pixels and objects into wood and non-wood categories. To train and validate the automatic detection process, a ground-truth or set of videos with manually annotations are required. Such annotations can be performed using different techniques. For example, objects can be identified with the help of a bounding box or selection of endpoints, as in MacVicar and Piégay(2012); Ghaffarian et al., (2020) and Zhang et al., (2020). It is also possible to sample wood pixels without specifying instances or objects, or to sample pixels within annotated objects. Finally, objects and/or pixels can be annotated multiple times in a video sequence to increase the amount and detail of information in such an annotation database. However, this annotation process is time-consuming, so a trade-off must be made between training and accuracy for different lighting conditions, camera parameters, wood properties, and river hydraulics.

Given that the tool is meant to be as flexible as possible, the annotation tool was developed to allow operator to perform as fine annotation as they wish. As it is shown in Fig 8, this module contains three main

parts: (i) The column on the far left allows operator to switch to another module (detection, learning or performance), (ii) the central part consists of a video player with a configuration tab for extracting the data, and (iii) the right part where the tools to generate, create, visualize and save annotations are located. The tools allow rather quick coarse annotation, similar to what was done by MacVicar and Piégay (2012) and Boivin *et al.*, (2015), while still allowing the possibility of finer pixel-scale annotation.

Fig 8

The principle of this module is to associate annotations with the frames of a given video. Annotating a piece of wood is like drawing its shape, directly on a frame of the video, using the drawing tools provided by the module. It is possible to add a text description to each annotation. Each annotation is linked to a single frame of the video; however, a frame can contain several annotations. An annotated video, therefore, consists of a video file, as well as a collection of drawings, possibly with textual descriptions, associated with frames. It is possible to link annotations from one frame to another to signify that they belong to the same piece of wood. These data can be used to learn the movement of pieces of wood in the frame.

3.3. Performance

The performance module allows the operator to set rules to compare automatic and manual wood detection results. This section also allows the operator to use a bare, pixel-based annotation or specify an orthorectification matrix to extract wood-size metrics directly from the output of an automatic detection.

For this module an automatic detection file is first loaded and then the result of this detection is compared with a manual annotation for that video, if the latter is available. Comparison results are then saved in the form of a summary file (*.csv format), allowing the operator to perform statistical analysis of the results or the performance of the detection algorithm. A manual annotation file can only be loaded if it is associated with an automatic detection result.

The performance of the detected algorithm can be realized on several levels:

- Object. The idea is to annotate one (or more) occurrences of a single object, and to operate the comparison at bounding box scale. A detected object may comprehend a whole sequence of occurrences, on several frames. It is validated when only a single occurrence happens to be related to an annotation. This is the minimum possible effort required to have an extensive overview of the object frequency on such an annotations database. This approach can however lead us to misjudge

overall wrongly detected sequences as True Positives (see below), or vice-versa.

- Occurrence. The idea is to annotate, even roughly, every occurrence of every woody object, so that the comparison can happen between bounding boxes rather than at pixel level. Every occurrence of any detected object can be validated individually. This option requires substantially more annotation work than the object annotation.
- Pixel. This case implies that every pixel of every occurrence of every object is annotated as wood. It is very powerful in the event of evaluating the algorithm performances, and eventually refining its parameters with the help of some machine learning technique. However, it requires an extensive annotation work.

4. Performance assessment

To assess the performance of the automatic detection algorithm, we used a set of videos from the Ain River in France that were both comprehensively manually annotated and automatically analyzed. According to the data annotated by the observer, the performance of the software can be affected by different conditions: (i) wood piece length, (ii) distance from the camera, (iii, iv) wood X, Y position, (v) flow discharge, (vi) daylight, and (vii, viii) light and darkness of the frame (see Table 2). If for example software detects a 1 cm piece at a distance of 100 m from the camera, there is a high probability that this is a false positive detection. Therefore, knowing the performance of the software in different conditions, it is possible to develop some rules to enhance the quality of data. The advantage of this approach is that all eight parameters introduced here are accessible easily in the detection process. In this section the monitoring details and annotation methods are introduced before the performance of the software is evaluated by comparing the manual annotations with the automatic detections.

Table 2

4.1. Material and methods

4.1.1. Monitoring site and annotation

The Ain River is a piedmont river with a drainage area of 3630 km^2 at the gauging station of Chazey-sur-Ain, with a mean flow width of 65 m, a mean slope of 0.15%, and a mean annual discharge of 120 m^3/s. The lower Ain River is characterized by an active channel shifting within a forested floodplain (Lassettre et al., 2008). An AXIS221 Day/Night^{TM} camera with a resolution of 768 × 576 pixels was installed at this station

to continuously record the water surface of the river at a maximum frequency of 5 fps (Fig 9). This camera replaced a lower resolution camera at the same location used by MacVicar and Piégay (2012). The specific location of the camera is on the outer bank of a meander, on the side closest to the thalweg, at a height of 9.8 m above the base flow elevation. The meander and a bridge pier upstream help to steer most of the floating wood so that it passes relatively close to the camera where it can be readily detected with a manual procedure (MacVicar and Piégay, 2012). The transformation matrix at the base flow elevation with the camera as the origin is shown in Fig 10. Straight lines near the edges of the image appear curved because the fisheye distortion has been corrected on this image (see Sect 2.3); conversely, a straight line, in reality, is presented without any curvature in the image.

Fig 9

Fig 10

The survey period examined on this river was during 2012 from which two flood events, (January 1-7 and December 15) were selected for annotation. A range of discharges from $400 m^3/s$ to $800\ m^3/s$ occurred during these periods (Fig 11), which is above a previously observed wood transport threshold of $\sim 300\ m^3/s$ (MacVicar and Piégay, 2012). The flow discharge is available from the website (*www.hydro.eaufrance.fr*). On January 3rd and 5*th*, a spider was active in front of the camera, which prevented a good video recording and these days were therefore removed from the database. Detection was only possible during the daylight. A summary of automated and manual detections for the six days is shown in Table 3.

Fig 11

4.1.2. Assessment Methodology

Ghaffarian et al. (2020), Zhang et al. (2020) show that the wood discharge can be measured from flux or frequency of wood objects. An object level detection was thus sufficient for the larger goals of this research at the Ain River, which is to get a complete budget of transported wood volume.

A comparison of annotated with automatic object detections gives rise to three options:

1- True Positive (TP): an object is correctly detected and is recorded in both the automatic and annotated database
2- False Positive (FP): an object is incorrectly detected and is recorded only in the automatic database.
3- False Negative (FN): an object is not detected automatically and is only recorded in the annotated

database.

Despite overlapping occurrences of wood objects in the two databases, the objects could vary in position and size between them. For the current study we set the TP threshold as the case where either at least 50% of the automatic and annotated bounding box areas were common or at least 90% of an automatic bounding box area was part of its annotated counterpart.

In addition to the raw counts of TPs, FPs, and FNs, we defined two measures of the performances of the application, where:

- Recall Rate (RR) is the fraction of wood objects that are automatically detected ($TP/(TP + FN)$); and
- Precision Rate (PR) is the fraction of detected objects that are wood ($TP/(TP + FP)$).

The higher the PR and the RR are, the more accurate our application is. However, both rates tend to interact. For example, it is possible to design an application that displays a very high RR (which means that it doesn't miss many objects), but suffers from a very low PR (it outputs a high amount of inaccurate data), and vice-versa. Thus, we have to find a balance that is appropriate to each application.

4.1.3. Factors used to understand variation in performance

It was well known from previous manual efforts to characterize wood pieces and develop automated detection tools that it is easier to detect certain wood objects than others. In general, the ability to detect the wood objects in the dynamic background of a river in flood was found to vary with the size of the wood object, its position in the image frame, the flow discharge, the amount and variability of the light, interference from other moving objects such as spiders, and other weather conditions such as wind and rain. In this section, we describe and define the metrics that were used to understand the variability of the detection algorithm performance.

In general, more light results in better detection. The light condition can be varied by variation of a set of factors such as weather conditions or amount of sediment which is carried by the river. In any case, the daylight is a factor that can change the light condition systematically, *i.e.* low light early in the morning (Fig 12.a), bright light at midday with potential for direct light and shadows (Fig 12.b), and low light again in the evening, though different from the morning because the hue is more bluish (Fig 12.c). This effect of the time of day was quantified simply by noting the time of the image, which was marked on the top of each frame of

394 the recorded videos.

Fig 12

395 Detection is also strongly affected by the frame 'roughness', defined here as the variation in light over
396 small distances in the frame. The change in light is important for the recognition of wood objects, but light
397 roughness can also occur when there is a region with relatively light pixels due to something such as reflection
398 of the surface of the water, and dark roughness can occur when there is a region with relatively dark pixels
399 due to something such as shadows from the surface water waves. Detecting wood is typically more difficult
400 around light roughness, which results in false negatives, while the color-map of a darker surface is often close
401 to that of wood, which results in false positives. Both of these conditions can be seen in Fig 12 which is
402 highlighted in Fig 12.a. In general, the frame roughness increases in windy days or when there is an obstacle
403 in the flow, such as downstream of the bridge pier in the current case. The light roughness was calculated for
404 the current study by defining a light intensity threshold and calculating the ratio of pixels of higher value
405 among the frame. The dark roughness is calculated in the same way, but in this case the pixels less than the
406 threshold were counted. In this work thresholds equal to 0.9 and 0.4 were used for light and dark roughness,
407 respectively.

408 The oblique view of the camera means that the distance of the wood piece from the camera is another
409 important factor in detection (Fig 13). The effect of distance on detection interacts with wood length, *i.e.*
410 shorter pieces of wood that are not detectable near the camera may not be detectable toward the far bank due
411 to the pixel size variation (Ghaffarian et al., 2020). Moreover, if a piece of wood passes through a region
412 with high roughness (Fig 13) or amongst bushes or trees (Fig 13 right hand side) it is more likely that the
413 software is unable to detect it. In our case, one day of video record could not be analyzed due to the presence
414 of a spider that moved around in front of the camera.

Fig 13

415 Flow discharge is another key variable in wood detection. Increasing flow discharge generally means
416 that water levels are higher, which brings wood close to the near bank of the river closer to the camera. This
417 change can make small pieces of wood more visible, but it also reduces the angle between the camera position
418 and pixels, which makes wood farther from the camera harder to see. High flows also tend to increase surface
419 waves and velocity, which can increase the roughness of the frame and lead to the wood being intermittently
420 submerged or obscured. More suspended sediment is carried during high flows which can change water

surface color and increase the opacity of the water.

4.2. Detection performance

Automatic detection software performance was evaluated based on the event based TP, FP, and FN raw numbers and the precision (PR) and recall rates (RR) using the default parameters in the software. On average, manual annotation resulted in the detection of approximately twice as many wood pieces as the detection software (Table 3). Measured over all the events, RR = 29%, which indicates that many wood objects were not detected by the software, while among detected objects about 36% were false detections ($PR = 64\%$).

Table 3

To better understand model performance, we first tested the correlation between the factors identified in the previous section (Table 4). As shown, the pairs of dark/light roughness, length/distance and discharge/time were highly correlated ($Corr. = 0.59, 0.46, 0.37$ respectively). For this reason, they were considered together to evaluate the performance of the algorithm within a given parameter space. The X/Y positions were also considered as a pair despite a relatively low correlation (0.15) because they represent the position of an object. As a note, the correlation between time and dark roughness is higher than discharge and time, but we used the discharge/time pair because discharge has a good correlation only with time. As recommended by MacVicar and Piégay (2012), wood lengths were determined on a log base 2 transformation to better compare different classes of floating wood, similar to what is done for sediment sizes.

Table 4
Fig 14

The presentation of model performance by pairs of correlated parameters clarifies certain strengths and weaknesses of the software (Figure 14). As expected, the results of Fig 14.b indicate that first, the software is not so precise for small pieces of wood (less than the order of 1 m), and second there is an obvious link between wood length and the distance from the camera so that by increasing the distance from the camera, the software is precise only for larger pieces of wood. Based on Fig 14.e, the software precision is usually better on the right side of the frame than the left side. It would be reasonable, as the software requires to detect a patch at least in 5 continuous frames to recognize it as a piece of wood (see Sect 2.2 and Fig 4 for more information). Therefore, most of the true positives are on the right side of the frame, where 5 continuous frames have already established. Also, the presence of the bridge pier (at X ≅ -30 to -40 m based on Fig 10)

in the upstream, produces lots of waves that decreases the precision of the software. Also, Fig 14.h shows that the software is much more precise during the morning when there is enough light rather than evening when the sunshine decreases. However, at low flow ($Q < 550\ m^3/s$) the software precision decreases significantly. Finally, based on Fig 14.k, the software does not work well in two roughness conditions: (i) in a dark smooth flow (light roughness $\cong 0$) when there are some dark patches (shadows) on the surface (dark roughness $\cong 0.3$), and (ii) when both roughness increases and there are many noises in a frame.

To estimate the fraction of wood pieces that the software did not detect, the recall rate RR is calculated in different conditions and a linear interpolation was applied on RR as it is presented in Fig 14, third column. According to Fig 14.c, RR is fully dependent on piece length so that for the lengths at the order of 10 m ($L = O(10)$) RR is very good. By contrast when $L = O(0.1{\sim}1)$ the RR is too small. There is a transient region when $L = O(1)$ which is slightly depends on the distance from the camera. One can say, the wood length is the most crucial parameter that affects the recall rate independent of the operator annotation. Based on Fig 14.f, the RR is much better on the left side of the frame than on the right side. It can be because the operator's eye needs some time to detect a piece of wood, so most of the annotations are on the right side of the frame. Having a small number of detections on the left side of the frame results in the small value of FN which followed by high values of RR in this region ($RR = TP/(TP + FN)$. Therefore, while the position of detection plays a significant role in the recall rate, it is completely dependent on the operator bias. By contrast, frame roughness, daytime, and flow discharge do not play a significant role in the recall rate (Fig 14. i, l).

4.3. Post-processing

This section is separated into two main parts. First, we show how to improve the precision of the software by a posteriori distinction between TP and FP. After removing FPs from the detected pieces, in the second part, we test a process to predict the annotated data that the software missed *i.e.* false negatives.

4.3.1. Precision improvement

To improve the precision of the automatic wood detection we first ran the software to detect pieces and extracted the eight key parameters for each piece as described in Sect 4.1.3. We then estimated the total precision of each object, as the average of four precisions from each sub-figure of Fig 14. In the current study the detected piece was considered to be a true positive if the total precision exceeded 50%. To check the validity of this process, we used cross-validation by leaving one day out, calculating the precision matrices based on five other days, and applying the calculated PR matrices on the day that was left out. As is seen in

Table 5, this post-processing step increases the precision of the software to 85%, an enhancement of 21%. The degree to which the precision is improved is dependent on the day left out for cross-validation. If, for example, the day left out had similar conditions to the mean, the PR matrices were well trained and were able to distinguish between TP and FP (*e.g.* 2nd Jan with 42% enhancement). On the other hand, if we have an event with new characteristics (*e.g.* very dark and cloudy weather or at discharges different from what we have in our database), the PR matrices were relatively blind and offered little improvement (*e.g.* 15th Dec with 10% enhancement).

Table 5

One difficulty with the post-processing reclassification of wood piece is that this new step can also introduce error by classifying real objects as false positives (making them a false negative) or vice-versa. Using the training data, we were able to quantify this error and categorized them as post-processed false negatives ($\boldsymbol{FN_{pp}}$) with an associated recall rate ($\boldsymbol{RR_{pp}}$). As shown in Table 5, the precision enhancement process lost only around 14% of TPs (RR_{pp}= 86%).

Instead of using all eight key parameters (four PR matrices) to calculate the overall precision, it is also possible to use other configurations by combining different matrices as it is shown in Fig 15. In this figure, the precision matrices 1 to 4 are the same as the matrices presented in Fig 14 and different colors show different combinations of these matrices. As it is seen, some configurations (e.g. (2,4) or (1,3,4)) result in better precision and some cases (e.g. (1,2) or (1,3)) there is almost no difference between post-processed PR and the raw data. The reason that configurations like (2,4) or (1,3,4) with a better precision rate were not used here was that in these cases the post-processed recall rate RR_{pp} was low (around 60%) meaning that by using these configurations many of true positives was removed. Therefore, to have the best precision enhancement with maximum post-processed recall rate all 4 different precision matrices are used (Fig 15, dark red scatters).

Fig 15

4.3.2. Modeling missed wood pieces based on the recall rate

The automated software detected 29% of the number of manually annotated wood pieces (Table 5). In the previous section, it was described how to enhance the precision of the software to ensure that these automatically detected pieces are TPs. The larger question, however, is how to model the missing pieces. Based on Fig 14, the software work well for very large objects in most areas of the image and in most lighting conditions. However, the smaller pieces were found to be harder to detect, making the wood length the most

503 important factor governing the recall rate. Based on this idea, the final step in the post processing is to apply
504 a model to account for the smaller wood pieces.

505 The model is based on the concept of a threshold piece length. Above the threshold, wood pieces are
506 likely to be accurately counting using the automatic software. Below the threshold, on the other hand, the
507 automatic detection software is likely to deviate from the manual counts. The actual length distribution was
508 first determined based on the manual annotations ($TP + FN$) (Fig 16.a). Also shown are the raw results of
509 the automatic detection software ($TP + FP$) and the raw results with the false positives removed (TP). At
510 this stage, the difference between the TP and the $TP + FN$ lines are the false negatives (FN) that the software
511 has missed. Comparison between the two lines shows that they tend to deviate between 2-3 m. The correla-
512 tion coefficient between them was calculated for thresholds varying from 1 cm to 15 m length and 2.5 m
513 length was defined as the optimum threshold length for recall modeling (Fig 16.b).

514 In the next step we wanted to estimate the pieces less than 2.5 m that the software missed. During the
515 automatic detection process, when the software detects a piece of wood, according to Fig 14 (third column),
516 the RR can be calculated for this piece (same protocol as precision enhancement in Sect 4.3.1). Therefore, if
517 for example the average recall rate for a piece of wood is 50%, there is likely to be another piece in the same
518 condition (defined by the eight different parameters described in Table 2) that the software could not detect.
519 To correct for these missed pieces, additional virtual pieces were added to the database. Fig 16.a, shows the
520 length distribution after adding these virtual pieces to the database (blue line, total of 5841 pieces). The result
521 shows a good agreement between this and the operator annotations (green line, total of 6249 pieces), which
522 results in a relative error of only 6.5% in the total number of wood pieces.

Fig 16

523 On the Ain River by separating videos to 15 min segments, MacVicar and Piégay, (2012) and Zhang et
524 al., (2020) proposed the following equation for calculating wood discharge from the wood flux:

525 $$Q_w = 0.0086F^{1.24} \quad (1)$$

526 where, Q_w is the wood discharge ($m^3/15min$) and F is the wood flux (piece number/15 min). Using
527 this equation, the total volume of wood was calculated based on three different conditions: (i) operator anno-
528 tation ($TP + FN$), (ii) raw data of the detection software ($TP + FP$) and (iii) post-processed data of the de-
529 tection software ($TP_{modeled}$). Fig 17 shows a comparison of the total volume of wood from the manual

annotations in comparison with the raw and post-processed annotations from the detection software. As shown, the raw detection results underestimate wood volume by almost one order of magnitude. After processing, the results show some scatter but are distributed around the 1:1 slope, which indicates that they follow the manual annotation results. There is a slight difference for days with lower fluxes (Jan 4 and 7), where the post-processing tends to over-estimate wood volumes, but in terms of an overall wood balance the volume of wood on these days are negligible. In total, 125 m^3 wood was annotated by the operator and the software automatically detected only 46 m^3, some of which represent false positives. After post-processing, 142 m^3 wood was estimated to have passed in the analyzed videos for a total error of 13.5%.

Fig 17

5. Conclusion

Here, we present new software for the automatic detection of wood pieces on the river surface. After presenting the corresponding algorithm and the user interface, an example of automatic detection was presented. We annotated 6 days of flood events that were used to first check the performance of the software and then develop post-processing steps to both remove possibly erroneous data and model data that were possibly missed by the software.

To evaluate the performance of the software, we used precision and recall rates. The automatic detection software detects around one third of all annotated wood pieces with 64% precision rate. Then using the operator annotations as the ultimate goal, the post-processing part was applied to extrapolate data extracted from detection results, aiming to come as close as possible to the annotations. It is shown that using four pair of key factors: (i) light and dark roughness of the frame, (ii) daytime and flow discharge, (iii) X, Y coordinates of detection position, and (iv) distance of detection as a function of piece length, it is possible to detect false positives and increase the software precision to 86%. Using the concept of a threshold piece length for detection it is shown that it is then possible to model the missed wood pieces (false negatives). In the presented results, the final recall rate results in a relative error of only 6.5% for piece number and 13.5% for wood volume.

This work shows the feasibility of the detection software to detect wood pieces automatically. Automation will significantly reduce the time and expertise required for manual annotation, making video monitoring a powerful tool for researchers and river managers to quantify the amount of wood in rivers. The

software should be applied in other rivers to test it in different contexts and enhance its accuracy.

6. Code/Data/Sample availability

Not available.

7. Author contribution

Hossein Ghaffarian: Application of statistical, and computational techniques to analyses study data. Creation and presentation of the published work.

Hervé Piégay, Bruce MacVicar, Hossein Ghaffarian: Development and design of methodology; creation of models.

Laure Tougne, Pierre Lemaire: Programming and software development.

Pierre Lemaire, Zhang Zhi: Performing the surveys, and data collection.

Hervé Piégay, Bruce MacVicar, Pierre Lemaire, Hossein Ghaffarian: Critical review, commentary, and revision.

Hervé Piégay: Oversight and leadership responsibility for the research activity planning and execution, including mentorship external to the core team.

8. Competing interests

The authors declare that they have no conflict of interest.

9. Acknowledgment

This work was performed within the framework and with the support of the PEPS (RiskBof Project (2016)) and LABEX IMU (ANR-10-LABX-0088) and within the framework of the EUR H2O'Lyon (ANR-17-EURE-0018) of Université de Lyon, le latter being both part of the program "Investissements d'Avenir" (ANR-11-IDEX-0007) operated by the French National Research Agency (ANR).

10. References

Abbe TB, Montgomery DR. 2003. Patterns and processes of wood debris accumulation in the Queets river basin, Washington. *Geomorphology* **51** : 81–107.

Ali I, Mille J, Tougne L. 2011. Wood detection and tracking in videos of rivers. In *Scandinavian Conference on Image Analysis*, pp. 646–655. Springer, Springer Berlin Heidelberg.

Ali I, Mille J, Tougne L. 2012. Space–time spectral model for object detection in dynamic textured background. *Pattern Recognition Letters* **33** : 1710–1716.

Ali I, Mille J, Tougne L. 2014. Adding a rigid motion model to foreground detection: application to moving object detection in rivers. *Pattern Analysis and Applications* **17** : 567–585.

Ali I, Tougne L. 2009. Unsupervised Video Analysis for Counting of Wood in River during Floods. *In Advances in Visual Computing*, Bebis G et al. (eds). Springer Berlin Heidelberg: Berlin, Heidelberg; 578–587.

Badoux A, Andres N, Turowski JM. 2014. Damage costs due to bedload transport processes in Switzerland. *Natural Hazards and Earth System Sciences (NHESS)* **14** (2), 279–294.

Benacchio V, Piégay H, Buffin-Bélanger T, Vaudor L. 2017. A new methodology for monitoring wood fluxes in rivers using a ground camera: Potential and limits. *Geomorphology* **279** : 44–58.

Benacchio V, Piégay H, Buffin-Belanger T, Vaudor L, Michel K. 2015. Automatioc imagery analysis to monitor wood flux in rivers (Rhône River, France). *Presented at the 2015 Third International Conference Wood In World Rivers*, 6 July, Padova, Italy. Available from: http://www.sedalp.eu/events/dwd/proceedings_WWR32015.pdf

Boivin M, Buffin-Bélanger T, Piégay H. 2015. The raft of the Saint-Jean River, Gaspé (Québec, Canada): A dynamic feature trapping most of the wood transported from the catchment. *Geomorphology* **231** : 270–280.

Boivin M, Buffin-Bélanger T, Piégay H. 2017. Interannual kinetics (2010–2013) of large wood in a river corridor exposed to a 50-year flood event and fluvial ice dynamics. *Geomorphology* **279** : 59–73.

603 Braudrick CA, Grant GE. 2000. When do logs move in rivers? *Water Resources Research* **36** : 571–
604 583.

605 Cerutti G, Tougne L, Mille J, Vacavant A, Coquin D. 2013. Understanding leaves in natural images–a
606 model-based approach for tree species identification. *Computer Vision and Image Understanding* **117** : 1482–
607 1501.

608 Cerutti G, Tougne L, Vacavant A, Coquin D. 2011. A parametric active polygon for leaf segmentation
609 and shape estimation. In *International symposium on visual computing*, pp. 202–213. Springer.

610 Comiti F, Andreoli A, Lenzi MA, Mao L. 2006. Spatial density and characteristics of woody debris in
611 five mountain rivers of the Dolomites (Italian Alps). *Geomorphology* **78** : 44–63.

612 De Cicco PN, Paris E, Ruiz-Villanueva V, Solari L, Stoffel M. 2018. In-channel wood-related hazards
613 at bridges: A review: In-channel wood-related hazards at bridges: A review. *River Research and Applications*
614 **34** : 617–628.

615 Ghaffarian H, Piégay H, Lopez D, Rivière N, MacVicar B, Antonio A, Mignot E. 2020. Video-moni-
616 toring of wood discharge: first inter-basin comparison and recommendations to install video cameras. Earth
617 Surface Processes and Landforms Available from: https://onlinelibrary.wiley.com/doi/abs/10.1002/esp.4875

618 Gordo A, Almazán J, Revaud J, Larlus D. 2016. Deep image retrieval: Learning global representations
619 for image search. In *European conference on computer vision*, pp. 241–257. Springer.

620 Gregory S, Boyer KL, Gurnell AM. 2003. Ecology and management of wood in world rivers. In *Amer-*
621 *ican Fisheries Society, Bethesda, USA*, , vol. 23, pp. 663–665.

622 Gurnell AM, Piégay H, Swanson FJ, Gregory SV. 2002. Large wood and fluvial processes. *Freshwater*
623 *Biology* **47** : 601–619.

624 Haga H, Kumagai T, Otsuki K, Ogawa S. 2002. Transport and retention of coarse woody debris in
625 mountain streams: An in situ field experiment of log transport and a field survey of coarse woody debris
626 distribution. *Water Resources Research* **38** : 1-1.

627 Jacobson PJ, Jacobson KM, Angermeier PL, Cherry DS. 1999. Transport, retention, and ecological

significance of woody debris within a large ephemeral river. *Journal of the North American Benthological Society* **18** : 429–444.

Keller EA, Swanson FJ. 1979. Effects of large organic material on channel form and fluvial processes. *Earth Surface Processes and Landforms* **4** : 361–380.

Kramer N, Wohl E. 2014. Estimating fluvial wood discharge using time-lapse photography with varying sampling intervals. *Earth Surface Processes and Landforms* **39** : 844–852.

Kramer N, Wohl E, Hess-Homeier B, Leisz S. 2017. The pulse of driftwood export from a very large forested river basin over multiple time scales, Slave River, Canada. *Water Resources Research* **53**(3) : 1928–1947.

Lagasse PF. 2010. Effects of debris on bridge pier scour, , vol. 653. Transportation Research Board

Lassettre NS, Piégay H, Dufour S, Rollet A-J. 2008. Decadal changes in distribution and frequency of wood in a free meandering river, the Ain River, France. *Earth Surface Processes and Landforms* **33** : 1098–1112.

Lejot J, Delacourt C, Piégay H, Fournier T, Trémélo M-L, Allemand P. 2007. Very high spatial resolution imagery for channel bathymetry and topography from an unmanned mapping controlled platform. *Earth Surface Processes and Landforms* **32** (11): 1705–1725.

Lemaire P, Piégay H, MacVicar B, Mouquet-Noppe C, Tougne L. 2014. Automatically monitoring driftwood in large rivers: preliminary results. *Presented at the 2014 AGU Fall Meeting*. 19 December, San Francisco, USA. Available from: https://agu.confex.com/agu/fm14/meetingapp.cgi/Paper/22487

Lienkaemper GW, Swanson FJ. 1987. Dynamics of large woody debris in streams in old-growth Douglas-fir forests. Canadian Journal of Forest Research **17** (2): 150–156.

Liu L, Ouyang W, Wang X, Fieguth P, Chen J, Liu X, Pietikäinen M. 2020. Deep learning for generic object detection: A survey. *International journal of computer vision* **128** : 261–318.

Lucía A, Comiti F, Borga M, Cavalli M, Marchi L. 2015. Dynamics of large wood during a flash flood in two mountain catchments. *Natural Hazards and Earth System Sciences* **15** (8): 1741.

Lyn D, Cooper T, Yi Y-K. 2003. Debris accumulation at bridge crossings: laboratory and field studies . Purdue University: West Lafayette. Available from: http://docs.lib.purdue.edu/jtrp/48

MacVicar B, Piégay H. 2012. Implementation and validation of video monitoring for wood budgeting in a wandering piedmont river, the Ain River (France). *Earth Surface Processes and Landforms* **37** (12): 1272–1289.

MacVicar BJ, Piégay H, Henderson A, Comiti F, Oberlin C, Pecorari E. 2009a. Quantifying the temporal dynamics of wood in large rivers: field trials of wood surveying, dating, tracking, and monitoring techniques. *Earth Surface Processes and Landforms* **34** (15): 2031–2046.

MacVicar BJ, Piégay H, Tougne L, Ali I. 2009b. Video monitoring of wood transport in a free-meandering piedmont river. In *AGU Fall Meeting Abstracts*.

Mao L, Comiti F. 2010. The effects of large wood elements during an extreme flood in a small tropical basin of Costa Rica. *WIT Transactions on Engineering Sciences* **67** : 225–236.

Marcus WA, Legleiter CJ, Aspinall RJ, Boardman JW, Crabtree RL. 2003. High spatial resolution hyperspectral mapping of in-stream habitats, depths, and woody debris in mountain streams. *Geomorphology* **55** (1-4): 363–380.

Marcus WA, Marston RA, Colvard Jr CR, Gray RD. 2002. Mapping the spatial and temporal distributions of woody debris in streams of the Greater Yellowstone Ecosystem, USA. *Geomorphology* **44** (3-4): 323–335.

Martin DJ, Benda LE. 2001. Patterns of Instream Wood Recruitment and Transport at the Watershed Scale. *Transactions of the American Fisheries Society* **130** (5): 940–958.

Mazzorana B, Ruiz-Villanueva V, Marchi L, Cavalli M, Gems B, Gschnitzer T, Mao L, Iroumé A, Valdebenito G. 2018. Assessing and mitigating large wood-related hazards in mountain streams: recent approaches. *Journal of Flood Risk Management* **11** (2): 207–222.

Moulin B, Piégay H. 2004. Characteristics and temporal variability of large woody debris trapped in a reservoir on the River Rhone(Rhone): implications for river basin management. *River Research and*

Applications **20** (1): 79–97.

Muste M, Fujita I, Hauet A. 2008. Large-scale particle image velocimetry for measurements in riverine environments. *Water Resources Research* **44** (W00D19)

Piégay H, Lemaire P, MacVicar B, Mouquet-Noppe C, Tougne L. 2014. Automatically monitoring driftwood in large rivers: preliminary results. In *AGU Fall Meeting Abstracts*.

Ravazzolo D, Mao L, Picco L, Lenzi MA. 2015. Tracking log displacement during floods in the Tagliamento River using RFID and GPS tracker devices. *Geomorphology* **228** : 226–233.

Roussillon T, Piégay H, Sivignon I, Tougne L, Lavigne F. 2009. Automatic computation of pebble roundness using digital imagery and discrete geometry. *Computers & Geosciences* **35** (10): 1992–2000.

Ruiz-Villanueva V, Bodoque JM, Díez-Herrero A, Bladé E. 2014. Large wood transport as significant influence on flood risk in a mountain village. *Natural hazards* **74** (2): 967–987.

Ruiz-Villanueva V, Bürkli L, Mazzorana B, Mao L, Ravazzolo D, Iribarren P, Wohl E, Nakamura F, Stoffel M. 2018. Defining and characterizing wood-laden flows in rivers using home videos. In *E3S Web of Conferences*, , vol. 40, p. 02014. EDP Sciences

Ruiz-Villanueva V, Piégay H, Gurnell AM, Marston RA, Stoffel M. 2016. Recent advances quantifying the large wood dynamics in river basins: New methods and remaining challenges: Large Wood Dynamics. *Reviews of Geophysics* **54** (3): 611–652.

Schenk ER, Moulin B, Hupp CR, Richter JM. 2014. Large wood budget and transport dynamics on a large river using radio telemetry. *Earth Surface Processes and Landforms* **39** (4): 487–498.

Senter, A.E., Pasternack, G.B., Piégay, H., Vaughan, M.C. & Lehyan, J.S. 2017 Wood export varies among decadal, annual, seasonal, and daily scale hydrologic regimes in a large, mediterranean climate, mountain river watershed. *Geomorphology* **276**, 164–179.

Senter AE, Pasternack GB. 2011. Large wood aids spawning Chinook salmon (Oncorhynchus tshawytscha) in marginal habitat on a regulated river in California. *River Research and Applications* **27** (5): 550–565.

Seo JI, Nakamura F. 2009. Scale-dependent controls upon the fluvial export of large wood from river catchments. *Earth Surface Processes and Landforms* **34** (6): 786–800.

Seo JI, Nakamura F, Chun KW. 2010. Dynamics of large wood at the watershed scale: a perspective on current research limits and future directions. *Landscape and Ecological Engineering* **6** (2): 271–287.

Seo JI, Nakamura F, Nakano D, Ichiyanagi H, Chun KW. 2008. Factors controlling the fluvial export of large woody debris, and its contribution to organic carbon budgets at watershed scales. *Water Resources Research* **44** (W04428)

Turowski JM, Badoux A, Bunte K, Rickli C, Federspiel N, Jochner M. 2013. The mass distribution of coarse particulate organic matter exported from an Alpine headwater stream. Earth surface dynamics **1** (1): 1–11.

Viola PA, Jones MJ. 2006. Object recognition system. US Patent 7,031,499.

Warren DR, Kraft CE. 2008. Dynamics of large wood in an eastern US mountain stream. Forest Ecology and Management **256** (4): 808–814.

Wohl E. 2013. Floodplains and wood. Earth-Science Reviews **123** : 194–212.

Wohl E, Scott DN. 2017. Wood and sediment storage and dynamics in river corridors. Earth Surface Processes and Landforms **42** (1): 5–23.

Zhang Z, Ghaffarian H, MacVicar B, Vaudor L, Antonio A, Michel K, Piégay H. 2020. Video monitoring of in-channel wood fluxes: critical events, flux prediciton and sampling window. *Earth Surface Processes and Landforms*

Table 1 Characteristics of streamside video monitoring techniques in different studies.

Article	Sampling	Temporal scales	Camera resolution	Study site
MacVicar & Piégay (2012)	15 min segments	3 floods/18 hr/5 fps	640 × 480	Ain, France
Kramer & Wohl (2014)	Total duration	32 days/12761 frames/0.017 fps	n/a	Slave, Canada
Boivin et al. (2017)	Total duration	3 floods/150 hr/25 fps	640 × 480	St Jean, Canada
Kramer et al. (2017)	Total duration	11 months/0.0017 fps	1268 × 760	Slave, Canada
Senter et al. (2017)	15 min segments	39 days/180 hr/4 fps	2048 × 1536	North Yuba, USA
Ghaffarian et al. (2020)	Total duration	2 floods/80 hr/1 fps	600 × 800	Isère, France
Zhang et al. (2020)	Total duration	7 floods & 1 windy period /183 hr/5 fps	from 640 × 480 up to 800 × 600	Ain, France

Table 2 Parameters used to assess the performance of the software

Parameter	Rational	Metric
Piece length	Larger objects are easier to detect.	Detecting an object in pixel coordinates. Transferring coordinates to metric. Calculating length, position, and distance.
Distance	Objects closer to the camera are easier to detect.	
X position	Some particular areas of turbulent flow in the field of view affect detection (e.g. presence of a bridge pier).	
Y position		
Discharge	Flow discharge affects water color, turbulence and the amount of wood.	Recorded water elevation data and calibrated rating curve at hydrologic station.
Time	Luminosity of the frames varies with time of day.	Time of day as indicated on top of each frame.
Dark roughness	Small spots with sharp contrast (either lighter or darker) affect detection.	% of pixels below an intensity threshold
Light roughness		% of pixels above an intensity threshold

723

Table 3 Summary of automated and manual detections

Date	discharge (m^3/s)		Water level (m)		Detection time (hr)	Number		Precision rate%	Recall rate%
	Q_{max}	Q_{min}	h_{max}	h_{min}		annot.	det.		
1/1/2012	718	633	-7.4	-7.8	7 to 17	2282	972	77	33
2/1/2012	772	674	-7.2	-7.6	7 to 17	802	380	52	24
4/1/2012	475	423	-8.4	-8.6	7 to 17	140	158	20	22
6/1/2012	786	763	-7.2	-7.2	7 to 17	712	384	54	29
7/1/2012	462	430	-8.5	-8.6	7 to 17	117	73	40	25
15/12/2012	707	533	-7.5	-8.2	9 to 14	1296	503	72	28
Total	786	423	-7.2	-8.6	55 hr	5349	2470	64	29

724

Table 4 Correlation between parameters

	Dark roughness	Light roughness	Length	Distance	X position	Y position	Discharge	Time
Dark roughness		0.59	-0.02	-0.04	0.04	0.1	0	0.57
Light roughness	0.59		-0.03	-0.03	0.03	0.09	-0.04	0.29
Length	-0.02	-0.03		0.46	-0.45	-0.35	-0.02	-0.01
Distance	-0.04	-0.03	0.46		-1	-0.16	0.14	-0.05
X position	0.04	0.03	-0.45	-1		0.15	-0.15	0.05
Y position	0.1	0.09	-0.35	-0.16	0.15		0	0.07
Discharge	0	-0.04	-0.02	0.14	-0.15	0		0.37
Time	0.57	0.29	-0.01	-0.05	0.05	0.07	0.37	

Table 5 Precision rate (PR) before and after post-processing

		1 Jan	2 Jan	4 Jan	6 Jan	7 Jan	15 Dec	Total
Raw data	TP	745	196	31	206	29	363	1570
	FP	227	184	127	178	44	140	900
	FN	1537	606	109	506	88	933	3779
	$PR\%$	77	52	20	54	40	72	64
	$RR\%$	33	24	22	29	25	28	29
Post-proc.	TP	658	150	30	178	22	315	1353
	FP	64	10	60	39	11	68	252
	FN_{pp}[1]	87	46	1	28	7	48	217
	$PR\%$	91	94	33	82	67	82	85
	RR_{pp}[2]%	88	77	97	86	76	87	86
PR improvement		14	42	13	28	27	10	21

[1] FN_{pp} denotes the false estimations of the precision matrices which results in missing some TP.

[2] RR_{pp} denotes the recall rate of post processing which corresponds to FN_{pp}.

731

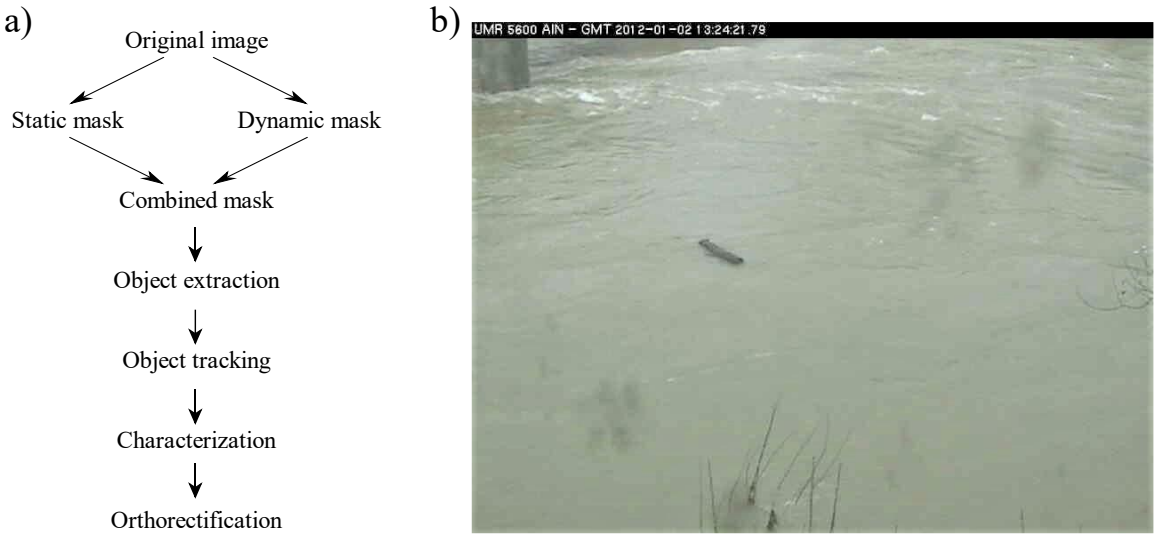

732

Fig 1 a) Flowchart of the detection software and b) an example of frame on which these different flowchart steps are applied.

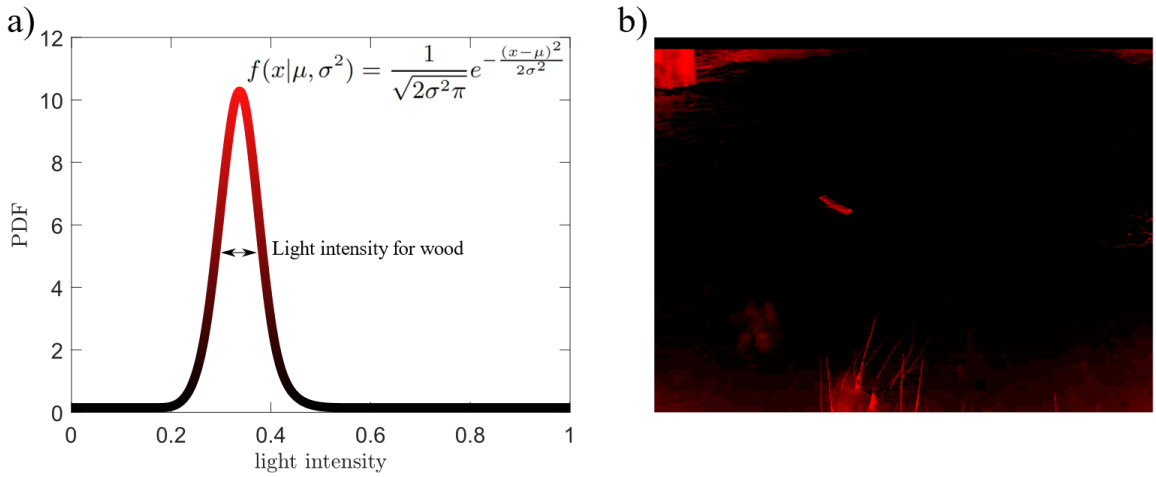

733

Fig 2 Static probability mask, a) Gaussian distribution of light intensity range for a piece of wood, b) employment of probability mask on the sample frame.

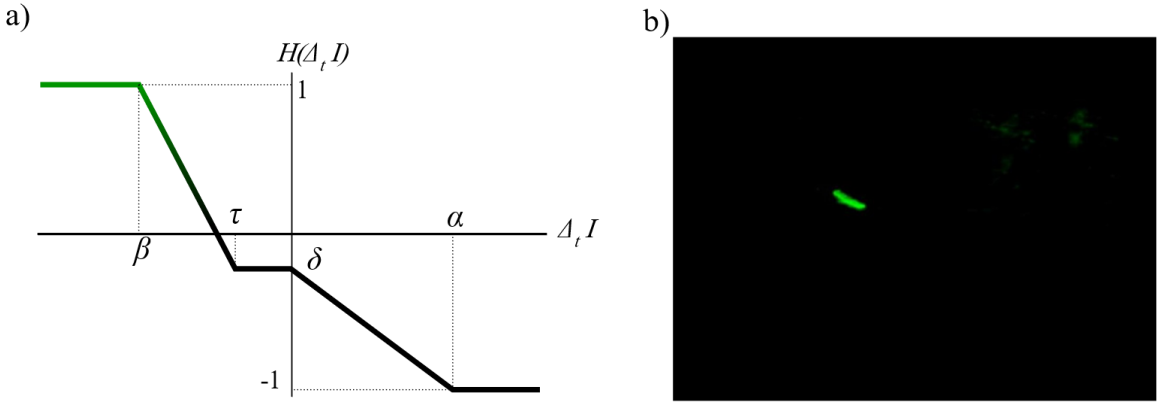

734

Fig 3 Dynamic probability mask, a) updating function $H(\Delta_t, I)$ adapted from Ali et al. (2011) and b) employment of probability mask on the sample frame.

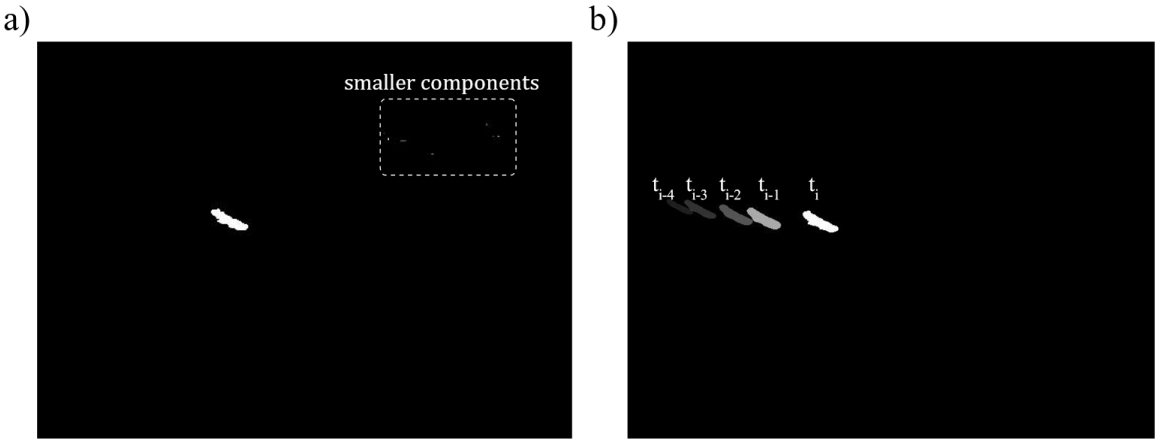

735

Fig 4 a) Object extraction by (i) combining static and dynamic masks and (ii) applying a threshold to retain only high-probability pixels. b) Object tracking as a filter to deal with partly immersed objects and to distinguish between moving objects from static waves.

736

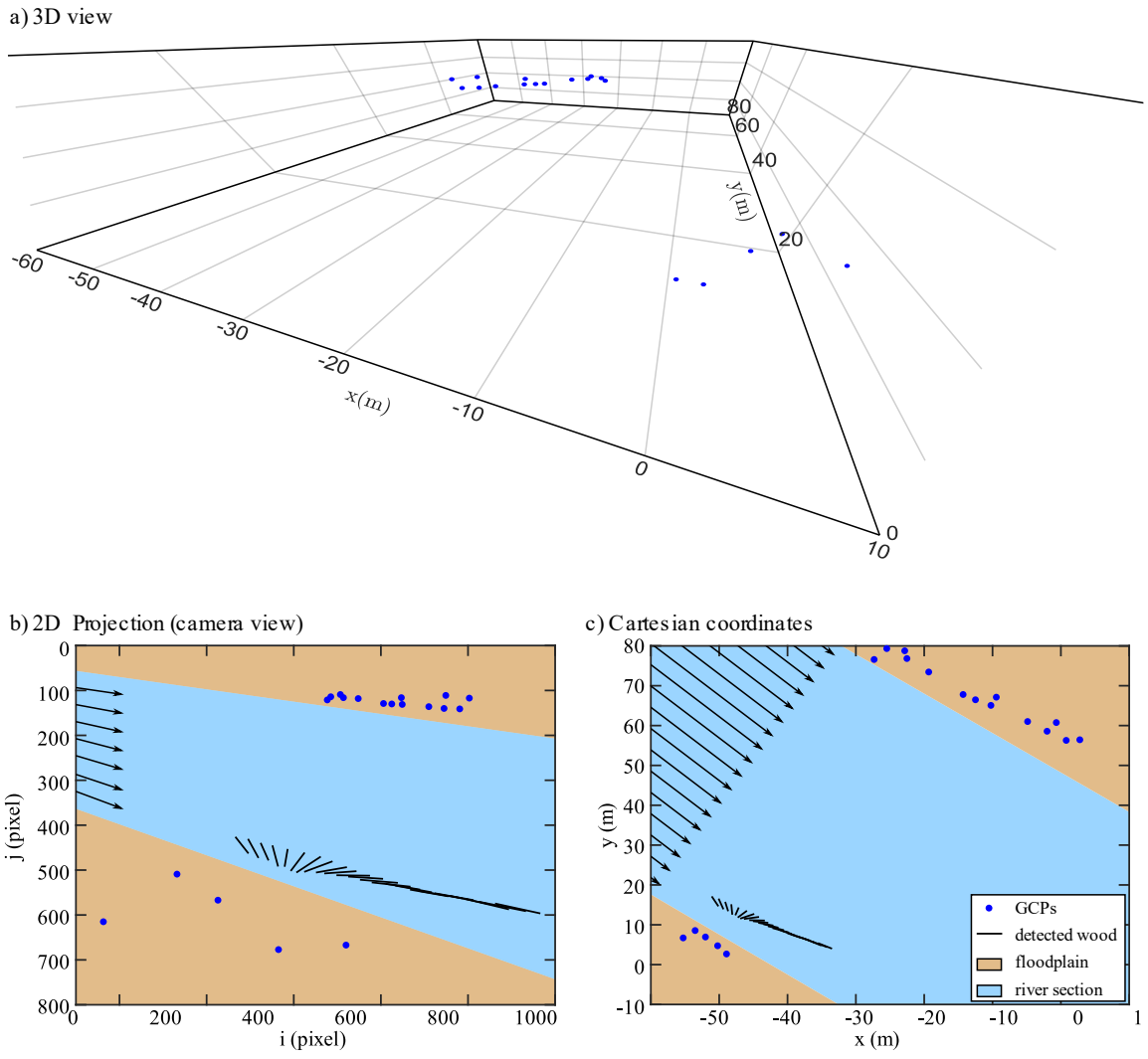

737

Fig 5 Image rectification, process. 3D view of non-colinear GCPs in metric coordinates (a), their corresponding localization within the image (b), and the relative 2D metric coordinates for a given water level (c). (b,c) A practical example of the transformation of the coordinates is presented. The different solid lines represent the successive detection in a set of consecutive frames.

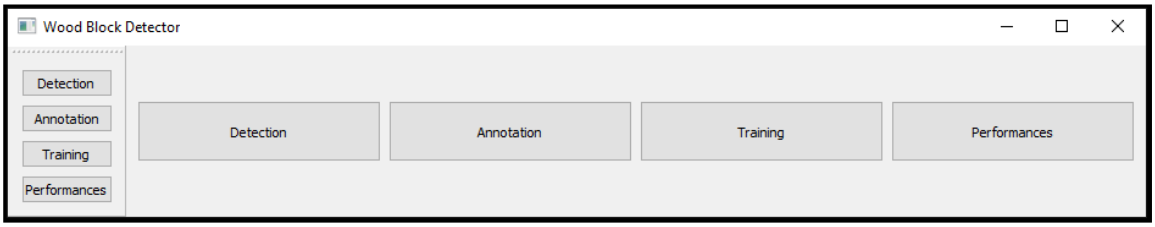

738

Fig 6 User interface of the detection software.

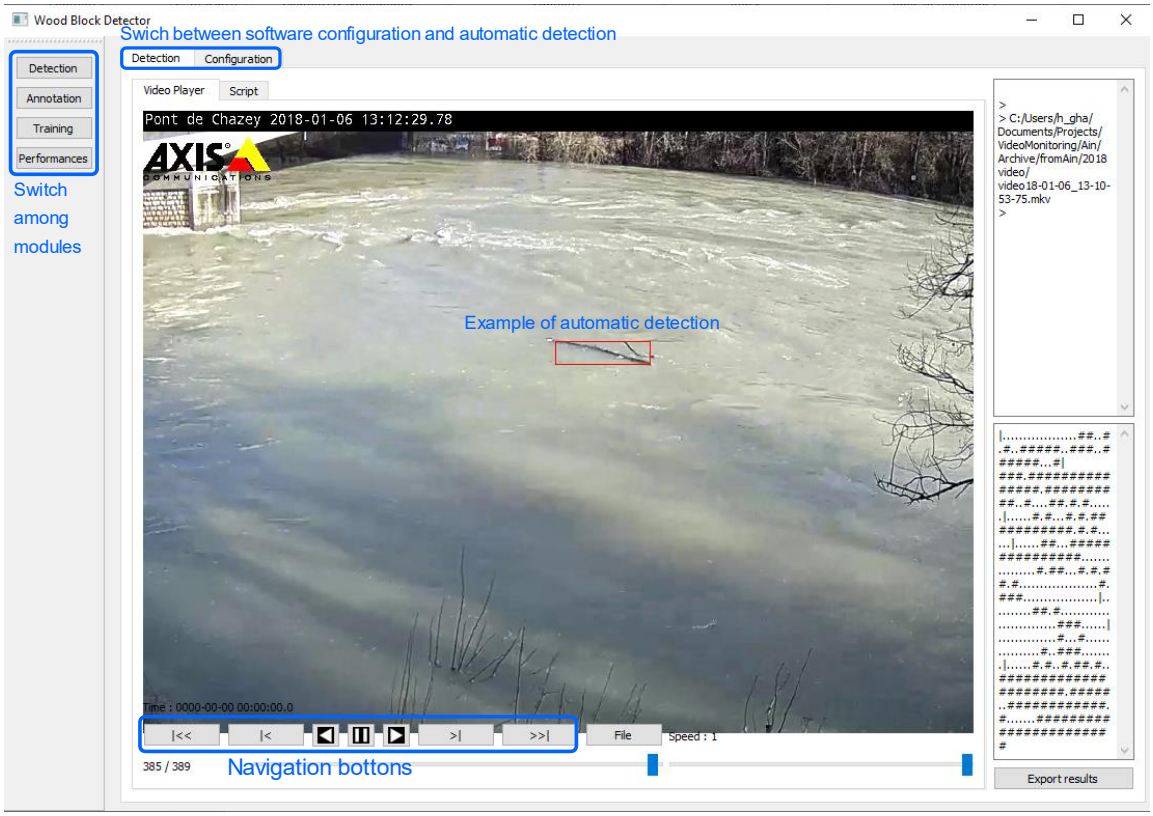

739

Fig 7 User interface of the detection module of automatic detection software.

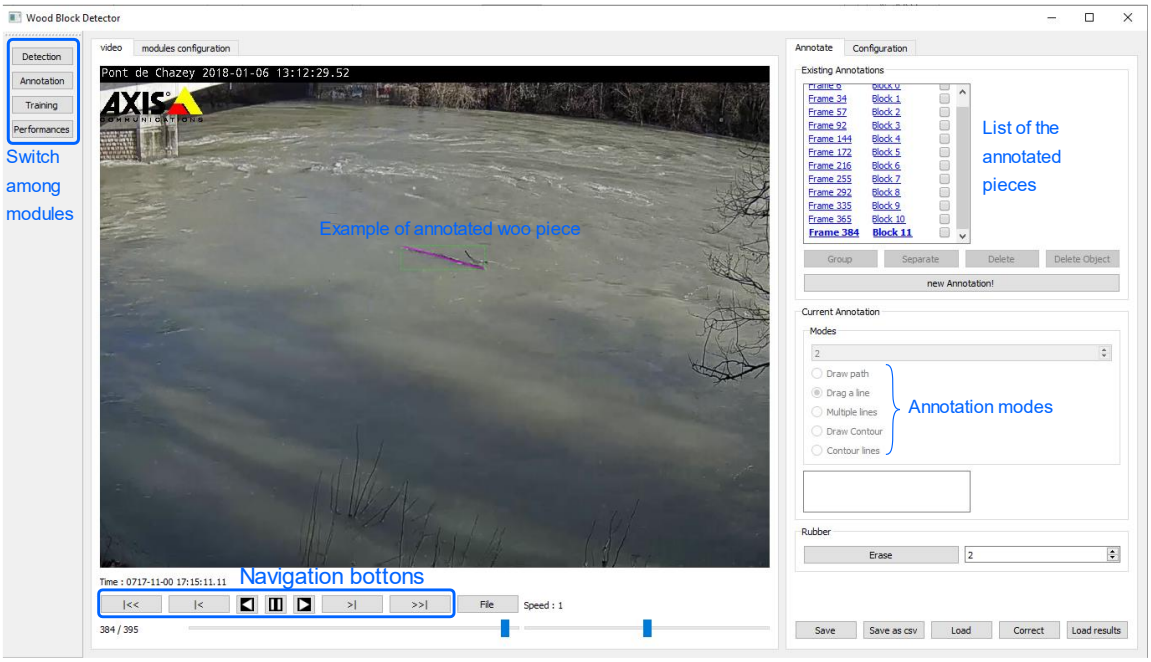

Fig 8 User interface of the annotation module of automatic detection software.

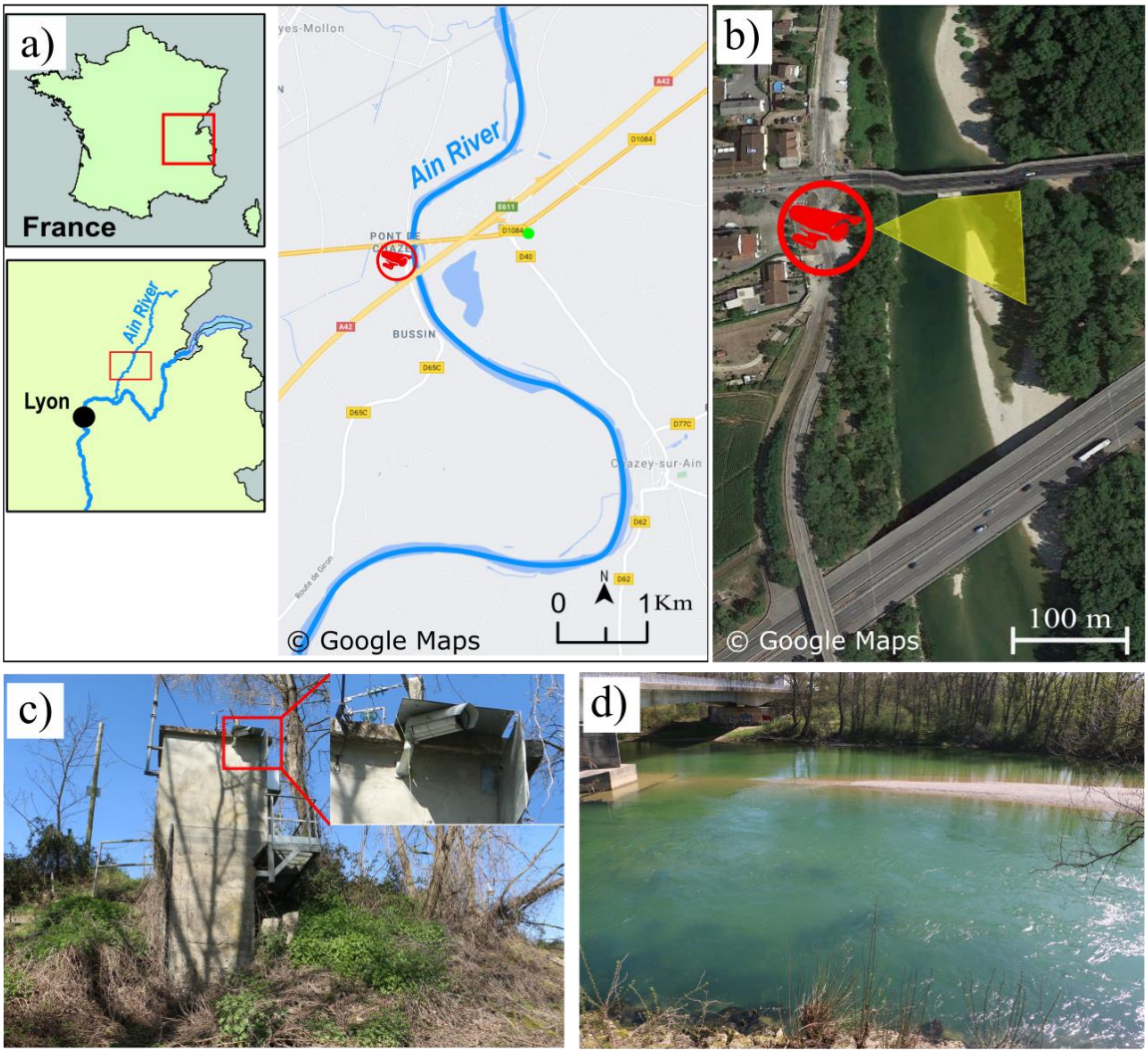

741 **Fig 9 Study site at Pont de Chazey: a) Location of the Ain River catchment in France and location of the gauging and meteorological stations, b) camera position and its view angle in yellow, c) overview of the gauging station with the camera installation point.**

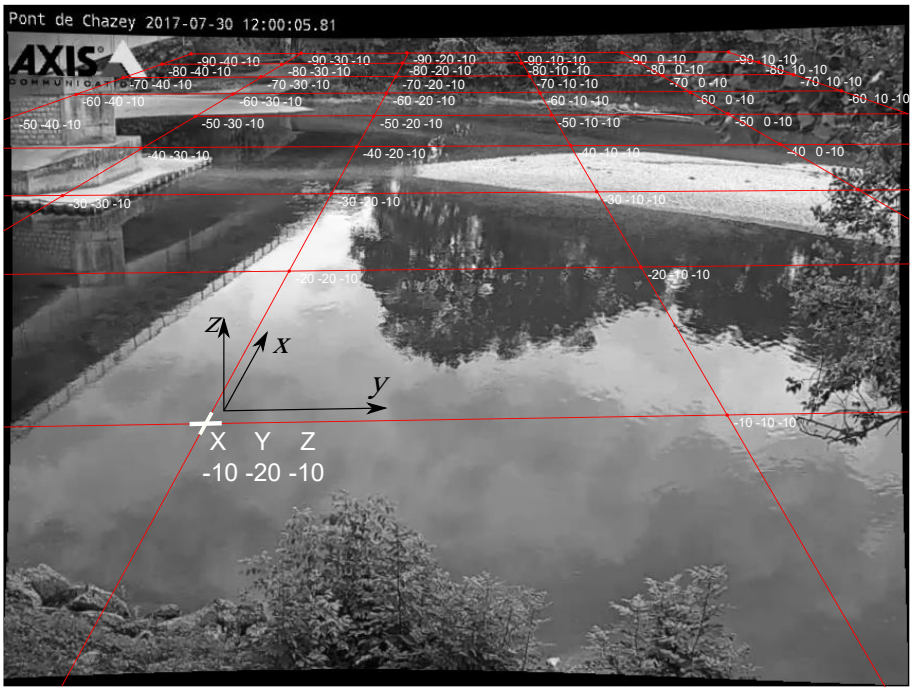

742

Fig 10 Rectifying transformation matrix at low flow level with camera at (0,0,0).

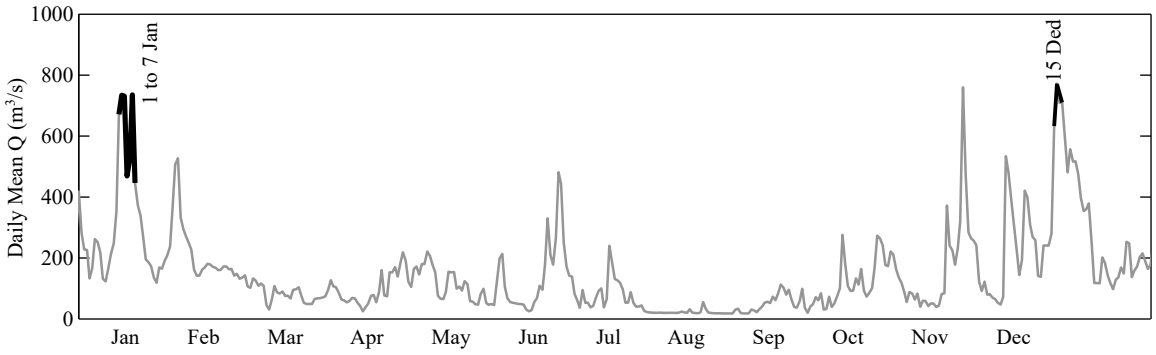

743

Fig 11 Daily mean discharge series for monitoring period from 1st to 7th January and in 15th December.

744

Fig 12 Different light conditions during (a) morning, (b) noon and (c) late afternoon, results in different frame roughness's and different detection performances.

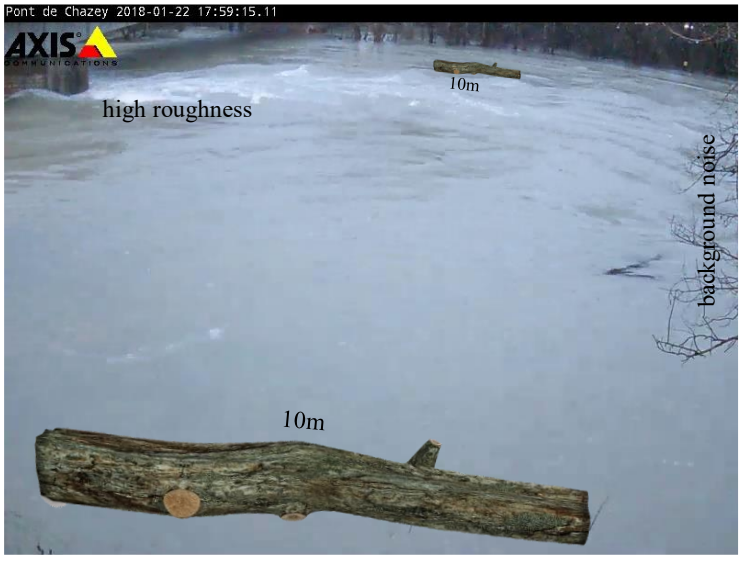

745

Fig 13 Wood position can highly affect the quality of detection. Pieces that are passing in front of the camera are detected much better than the pieces far from the camera.

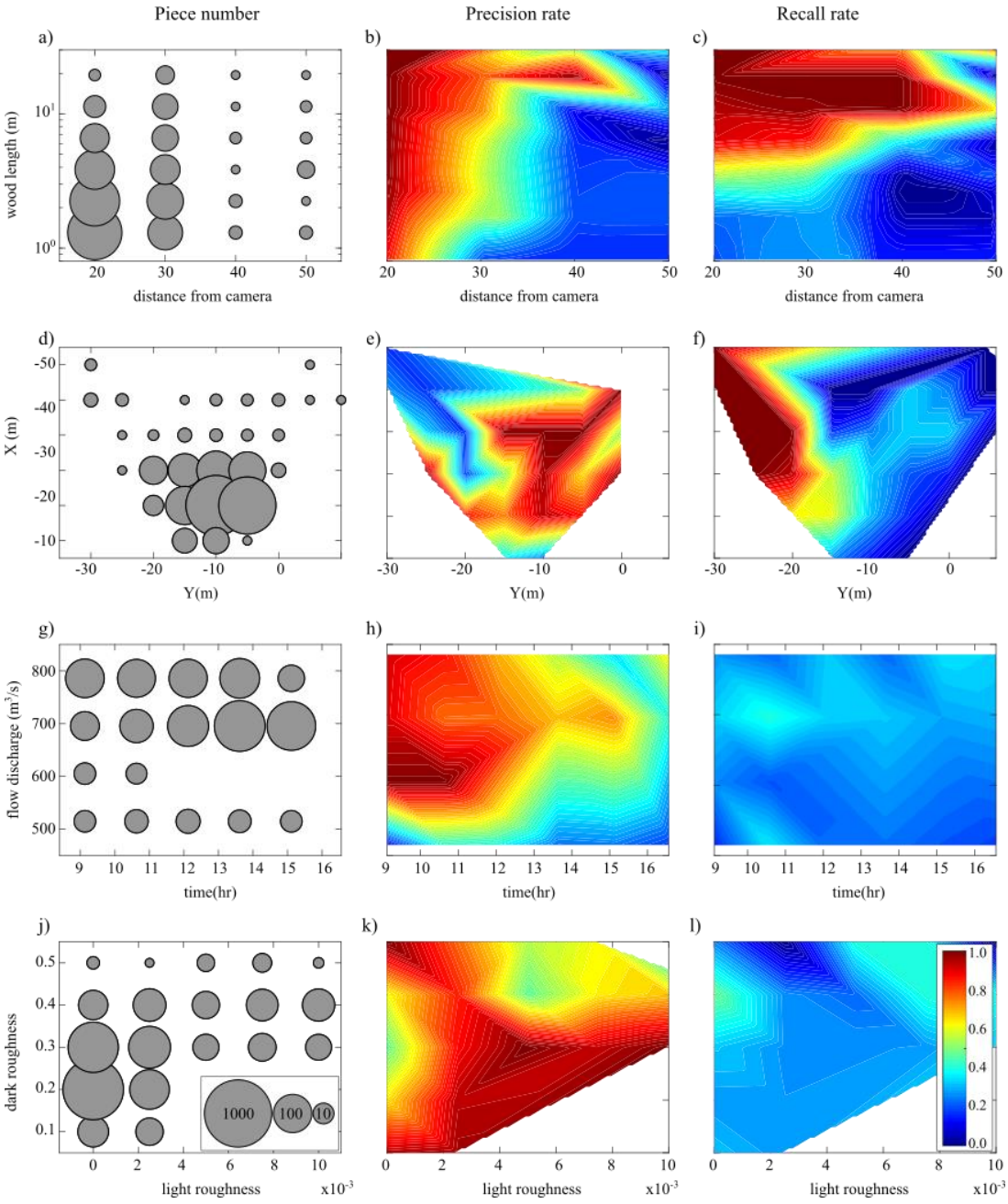

746

Fig 14 Correction matrices: a, b, c) wood lengths as a function of the distance from the camera, d, e, f) detection position, g, h, i) flow discharges during the daytime, and j, k, l) light and dark roughness's. The first column shows number of all annotated pieces. Second and third columns show Precision and Recall rates of the software respectively.

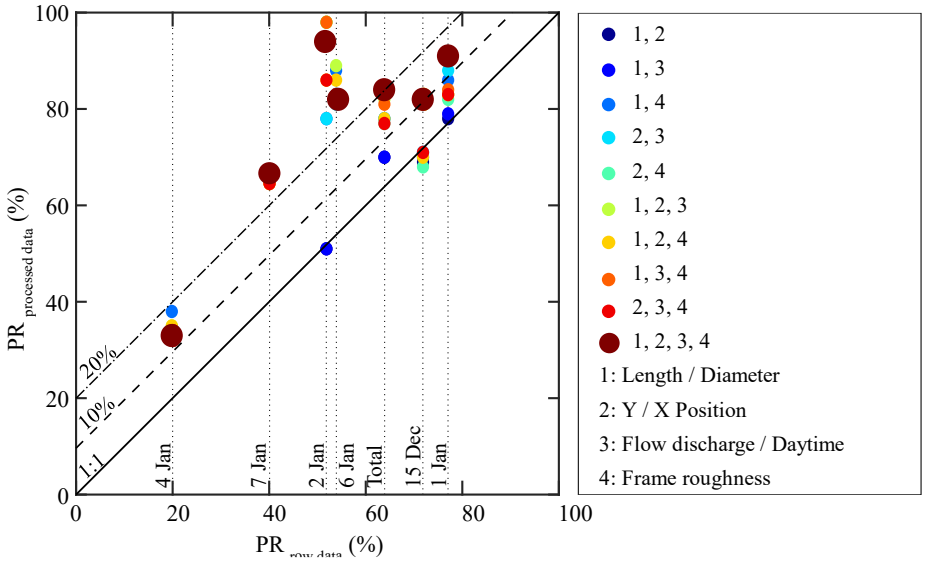

747

Fig 15 Effect of using different combinations of PR matrices on precision improvement compared with 1:1 line(no improvement), 10% and 20% improvement lines.

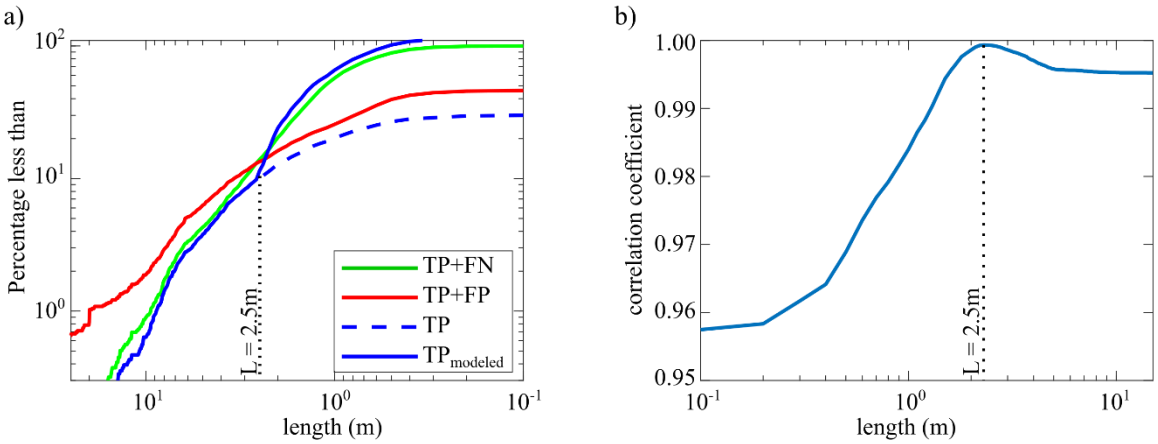

748

Fig 16 a) Steps to post-process software automatic detections: (i) raw detections ($TP + FP$ red line), (ii) Only true positives using the PR improvement process (TP blue dashed line), and (iii) modeling false negatives (blue line). Operator annotation (green line is used as a benchmark). b) The correlation coefficient between operator annotation and modeled TP to find an optimum threshold length for RR improvement.

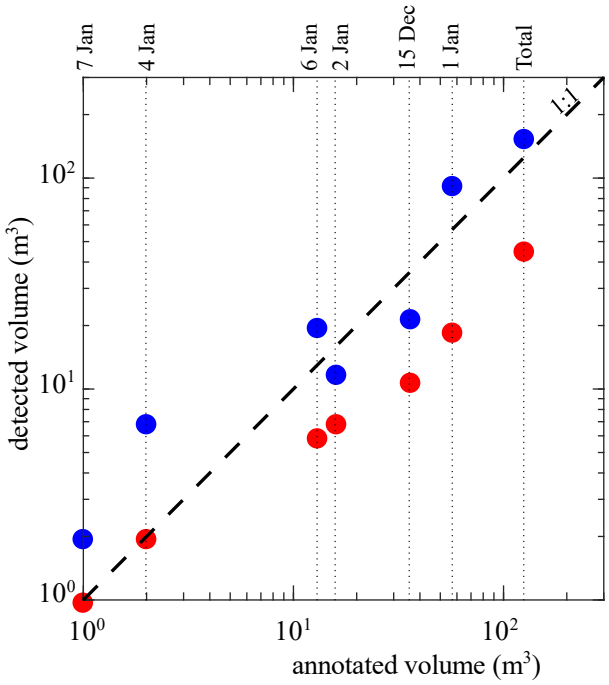

749

Fig 17 Comparison of the total volume of wood between operator annotation as the benchmark and raw data (red scatters) and post-processed data (blue scatters), compared with a 1:1 line.